

perience correlate with subsequent choices offers strong evidence for the existence of intrinsic preferences. Although it is not clear how malleable these preferences are, their existence may have health implications for the way in which individuals deal with events that are known to be unpleasant—for example, going to the doctor for painful procedures. The neurobiological mechanisms governing dreading behavior may hold clues for both better pain management and improvements in public health.

References and Notes

1. P. A. Samuelson, *Rev. Econ. Stud.* **4**, 155 (1937).
2. The opposite of utility is generally referred to as disutility, but for the sake of clarity, we refer to “utility” as possessing both positive and negative domains.
3. G. Loewenstein, *Econ. J.* **97**, 666 (1987).
4. A. Caplin, J. Leahy, *Q. J. Econ.* **116**, 55 (2001).
5. R.-R. Ji, T. Kohno, K. A. Moore, C. J. Woolf, *Trends Neurosci.* **26**, 696 (2003).
6. A. Ploghaus *et al.*, *Science* **284**, 1979 (1999).
7. T. Koyama, J. G. McHaffie, P. J. Laurienti, R. C. Coghill, *Proc. Natl. Acad. Sci. U.S.A.* **102**, 12950 (2005).
8. T. T. Raji, J. Numminen, S. Narvanen, J. Hiltunen, R. Hari, *Proc. Natl. Acad. Sci. U.S.A.* **102**, 2147 (2005).

9. I. Tracey, *Curr. Opin. Neurobiol.* **15**, 478 (2005).
10. A. D. Craig, *Annu. Rev. Neurosci.* **26**, 1 (2003).
11. R. Peyron, B. Laurent, L. Garcia-Larrea, *Neurophysiol. Clin.* **30**, 263 (2000).
12. Materials and methods are available as supporting material on Science Online.
13. H. R. Varian, *Intermediate Microeconomics: A Modern Approach* (Norton & Co., New York, ed. 6, 2002).
14. K. C. Berridge, in *Well-Being. The Foundations of Hedonic Psychology*, D. Kahneman, E. Diener, N. Schwarz, Eds. (Russell Sage Foundation, New York, 1999), pp. 525–557.
15. P. Petrovic, K. M. Petersson, P. Hansson, M. Ingvar, *Neuroimage* **16**, 1142 (2002).
16. B. A. Vogt, *Nat. Rev. Neurosci.* **6**, 533 (2005).
17. D. E. Bentley *et al.*, *Clin. Neurophysiol.* **115**, 1846 (2004).
18. D. E. Bentley, S. W. G. Derbyshire, P. D. Youell, A. K. P. Jones, *Pain* **102**, 265 (2003).
19. E. A. Phelps, *Annu. Rev. Psychol.* **57**, 27 (2006).
20. P. Rainville, B. Carrier, R. K. Hofbauer, M. C. Bushnell, G. H. Duncan, *Pain* **82**, 159 (1999).
21. S. M. McClure, D. I. Laibson, G. Loewenstein, J. D. Cohen, *Science* **306**, 503 (2004).
22. D. Kahneman, P. P. Wakker, R. Sarin, *Q. J. Econ.* **112**, 375 (1997).
23. C. Camerer, G. Loewenstein, D. Prelec, *J. Econ. Lit.* **43**, 9 (2005).
24. R. A. Rescorla, A. R. Wagner, in *Classical Conditioning 2: Current Research and Theory*, A. H. Black, W. F. Prokasy, Eds.

- (Appleton Century-Crofts, New York, 1972), pp. 64–69.
25. R. S. Sutton, *Mach. Learn.* **3**, 9 (1988).
26. C. K. Morewedge, D. T. Gilbert, T. D. Wilson, *Psychol. Sci.* **16**, 626 (2005).
27. A. Ploghaus *et al.*, *Proc. Natl. Acad. Sci. U.S.A.* **97**, 9281 (2000).
28. A. Ploghaus, L. Becerra, C. Borras, D. Borsook, *Trends Cogn. Sci.* **7**, 197 (2003).
29. T. V. Salomons, T. Johnstone, M.-M. Backonja, R. J. Davidson, *J. Neurosci.* **24**, 7199 (2004).
30. T. D. Wager *et al.*, *Science* **303**, 1162 (2004).
31. C. A. Porro *et al.*, *J. Neurosci.* **22**, 3206 (2002).
32. A. Ferretti *et al.*, *Neuroimage* **23**, 1217 (2004).
33. U. Bingel *et al.*, *Neuroimage* **23**, 224 (2004).
34. We thank C. M. Capra, C. Noussair, A. Rangel, and A. Rustichini for comments on this paper. Supported by grants from the National Institute on Drug Abuse (DA00367 and DA016434).

Supporting Online Material

www.sciencemag.org/cgi/content/full/312/5774/754/DC1
Materials and Methods
Figs. S1 to S6
Tables S1 to S3
References

12 December 2005; accepted 17 March 2006
10.1126/science.1123721

Conjunctive Representation of Position, Direction, and Velocity in Entorhinal Cortex

Francesca Sargolini,¹ Marianne Fyhn,¹ Torkel Hafting,¹ Bruce L. McNaughton,^{1,2} Menno P. Witter,^{1,3} May-Britt Moser,¹ Edvard I. Moser^{1*}

Grid cells in the medial entorhinal cortex (MEC) are part of an environment-independent spatial coordinate system. To determine how information about location, direction, and distance is integrated in the grid-cell network, we recorded from each principal cell layer of MEC in rats that explored two-dimensional environments. Whereas layer II was predominated by grid cells, grid cells colocalized with head-direction cells and conjunctive grid \times head-direction cells in the deeper layers. All cell types were modulated by running speed. The conjunction of positional, directional, and translational information in a single MEC cell type may enable grid coordinates to be updated during self-motion-based navigation.

The MEC is the hub of a widespread brain network for spatial navigation (1–11). Layer II of the MEC contains a two-dimensional (2D), ensemble-encoded metric map of relative spatial location (6–8) that is independent of the specific environment and the external sensory cues (7, 11). The elements of the map are “grid” cells, which fire whenever the animal’s position coincides with the

vertices of a periodic triangular grid spanning the complete surface of the environment, with different cells having different firing coordinates on the unit grid (7, 12). The regular structure of the grid field, and the environmentally invariant relationships among simultaneously recorded grid fields (13), implicates the grid cell as part of a universal, path-integration-based spatial metric, but its interaction with other cell types in MEC is not understood. To investigate the integration of metric spatial information in the multilayered entorhinal network (10, 14, 15), we compared the activity of cell populations in its four principal cell layers while rats were running in a 2D environment (16). Recordings were made from the most dorsal 23% of MEC in 17 rats (Fig. 1).

Grid cells with tessellating firing fields (7) were observed in all principal cell layers (Fig. 1, A and B). To compare their prevalence, we estimated the periodicity of the rate map of each cell by computing a 2D autocorrelation matrix for the rate distribution (Fig. 1C, left), rotating the autocorrelation map in steps of 6°, and calculating the correlation between each rotated map and the original. Grid structure was apparent as a sinusoidal modulation of this correlation, with peaks recurring at multiples of 60° (Fig. 1C, right, and fig. S1) (12). The degree of “gridness” was expressed as the difference between the correlations at the expected peaks (60° and 120°) and the expected troughs (30°, 90°, and 150°) of the function. The proportion of cells with a sinusoidal modulation was layer-dependent (Fig. 1D and table S1). Whereas most well-separated layer II cells had strongly periodic firing fields, only a smaller proportion of the deeper neurons had such characteristics; however, the range of “gridness” among those cells was not different from that of the layer II cells.

To compare the geometric structure of grids in different layers, we defined grid cells as the subset of cells that had higher correlations at 60° and 120° of rotation than at 30°, 90°, and 150° (gridness > 0) (16). All 203 neurons that passed this criterion had stable periodic firing patterns both within and between trials (figs. S1 and S2). Irrespective of layer, the scale of the grid in these cells increased by a factor of 1.5 to 2 from the dorsalmost to the ventralmost recording location, such that cells near the postrhinal border had the densest spacing (~35 to 40 cm) and the smallest firing fields (~500 cm²) (fig. S3). The correlations between distance from the

¹Centre for the Biology of Memory, Norwegian University of Science and Technology, 7489 Trondheim, Norway. ²Arizona Research Laboratories Division of Neural Systems, Memory, and Aging, University of Arizona, Tucson, AZ 85724, USA. ³Research Institute Neurosciences, Department of Anatomy and Neurosciences, Vrije Universiteit University Medical Center, Amsterdam, Netherlands.

*To whom correspondence should be addressed. E-mail: edvard.moser@ntnu.no

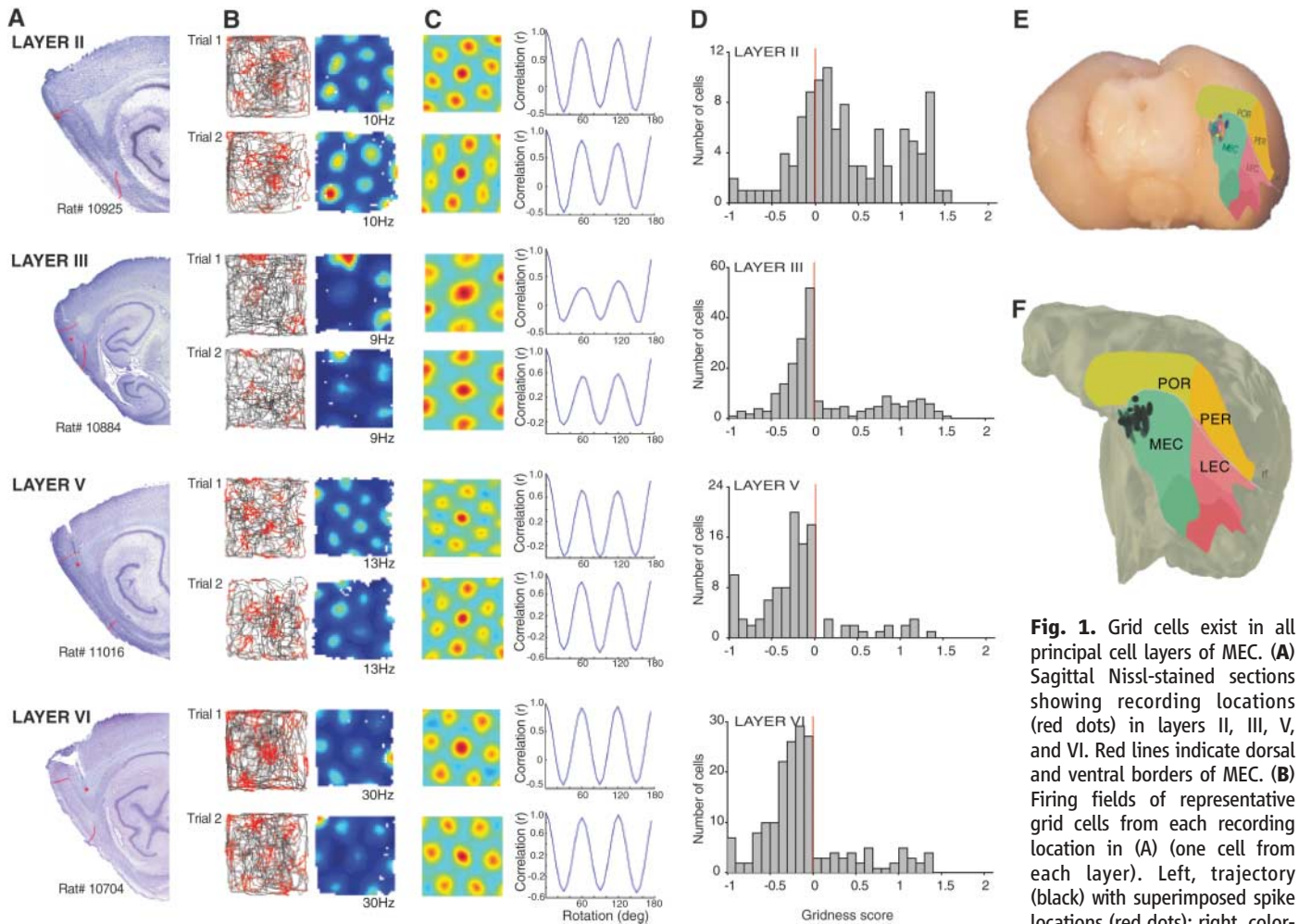


Fig. 1. Grid cells exist in all principal cell layers of MEC. **(A)** Sagittal Nissl-stained sections showing recording locations (red dots) in layers II, III, V, and VI. Red lines indicate dorsal and ventral borders of MEC. **(B)** Firing fields of representative grid cells from each recording location in (A) (one cell from each layer). Left, trajectory (black) with superimposed spike locations (red dots); right, color-coded rate map with the peak rate indicated. Red is maximum, dark blue is zero. Pixels not covered are white. Spike activity was recorded during two trials of running in a square box (10 min each, 10 min interval). **(C)** Periodic firing structure of the grid cells shown in (B). Left, autocorrelation matrix for the rate map. The color scale is from blue ($r = -1$) through green ($r = 0$) to red ($r = 1$). The distance scale of the autocorrelogram is the same as for the rate map; only the central part of the autocorrelogram is shown. Right, periodicity of the autocorrelation matrix. We rotated the autocorrelation map in steps of 6° and computed the correlation between each rotated map and the original. Correlations are 1 at 180° because of the mirror symmetry of the autocorrelation matrix. **(D)** Frequency distribution of gridness for all cells recorded in all cell layers of the MEC. **(E)** Ventral-posterior view of a whole rat brain, indicating the position of the reconstructed region in (F). The orientation of the brain in (E) and (F) is similar. **(F)** Three-dimensional reconstruction of the posterolateral surface of one hemisphere showing the complete range of recording locations in all 17 animals. For each animal, the position and dorsoventral extent of the tetrode tract is indicated as a black ellipsoid. Note clustering of recording locations in the most dorsomedial quarter (23%) of the MEC (dark and light green), with the majority of tetrodes positioned in the dorsal 5 to 15%. Recording locations were clustered dorsally for the practical reason that, at deeper levels, the grid scale becomes too large for quantitative analysis given the limited size of the apparatus. LEC, lateral entorhinal cortex; POR, postrhinal cortex; PER, perirhinal cortex; gray line, rhinal fissure (rf). Subdivisions of MEC (green) and LEC (red) are indicated by light and dark colors.

postprhinal border on the one hand and spacing and field size on the other were significant in all layers (spacing, $0.46 \leq r \leq 0.94$; field size, $0.44 \leq r \leq 0.94$; all, $P < 0.005$) (17). In all layers, the phase of the grid was distributed, i.e., the vertices of most nearby grid cells were offset relative to each other, but the orientation of the grids was consistent across all simultaneously recorded cells.

Beneath layer II, grid cells were colocalized with head-direction cells whose general properties were similar to those of head-direction cells in other brain areas (18–21) (Fig. 2). In these neurons, firing increased from a low background rate (typically < 0.5 Hz) to a high maximum rate (5 to 40 Hz) whenever the rat's head faced a certain range of directions (Fig. 2D, fig. S4, and table S1). The preferred firing direction varied among cells. The degree of directional tuning was quantified for each cell by comparing the distribution of the rat's orientation at the time of firing with the distribution of orientations across the entire trial, using Watson's U^2 test statistic (20). When these distributions differed significantly and the directional bias was significantly correlated across blocks of the trial, the cell was classified as a head-direction cell. No head-direction cells were found in layer II (Fig. 2E). In contrast, a large proportion of the cells in layers III to VI had directional

preferences (273 of 385 cells) (Fig. 2E). The breadth of tuning was not significantly different between layers III, V, and VI (mean U^2 values, 18.2, 25.2, and 18.3, respectively; mean angular standard deviations, 55.9° , 52.2° , and 58.2° ; $P > 0.05$) (fig. S4). The entire range of head directions was represented in all three layers (Fig. 2F). When several head-direction cells were recorded simultaneously in the same area, their peak firing directions were widely distributed (Fig. 2G and fig. S5). Head-direction cells were usually encountered together with grid cells (fig. S6). Directional tuning curves were always stable across trials (circular correlation, $r = 0.84$, $P < 0.001$).

preferences (273 of 385 cells) (Fig. 2E). The breadth of tuning was not significantly different between layers III, V, and VI (mean U^2 values, 18.2, 25.2, and 18.3, respectively; mean angular standard deviations, 55.9° , 52.2° , and 58.2° ; $P > 0.05$) (fig. S4). The entire range of head directions was represented in all three layers (Fig. 2F). When several head-direction cells were recorded simultaneously in the same area, their peak firing directions were widely distributed (Fig. 2G and fig. S5). Head-direction cells were usually encountered together with grid cells (fig. S6). Directional tuning curves were always stable across trials (circular correlation, $r = 0.84$, $P < 0.001$).

www.sciencemag.org **SCIENCE** VOL 312 5 MAY 2006

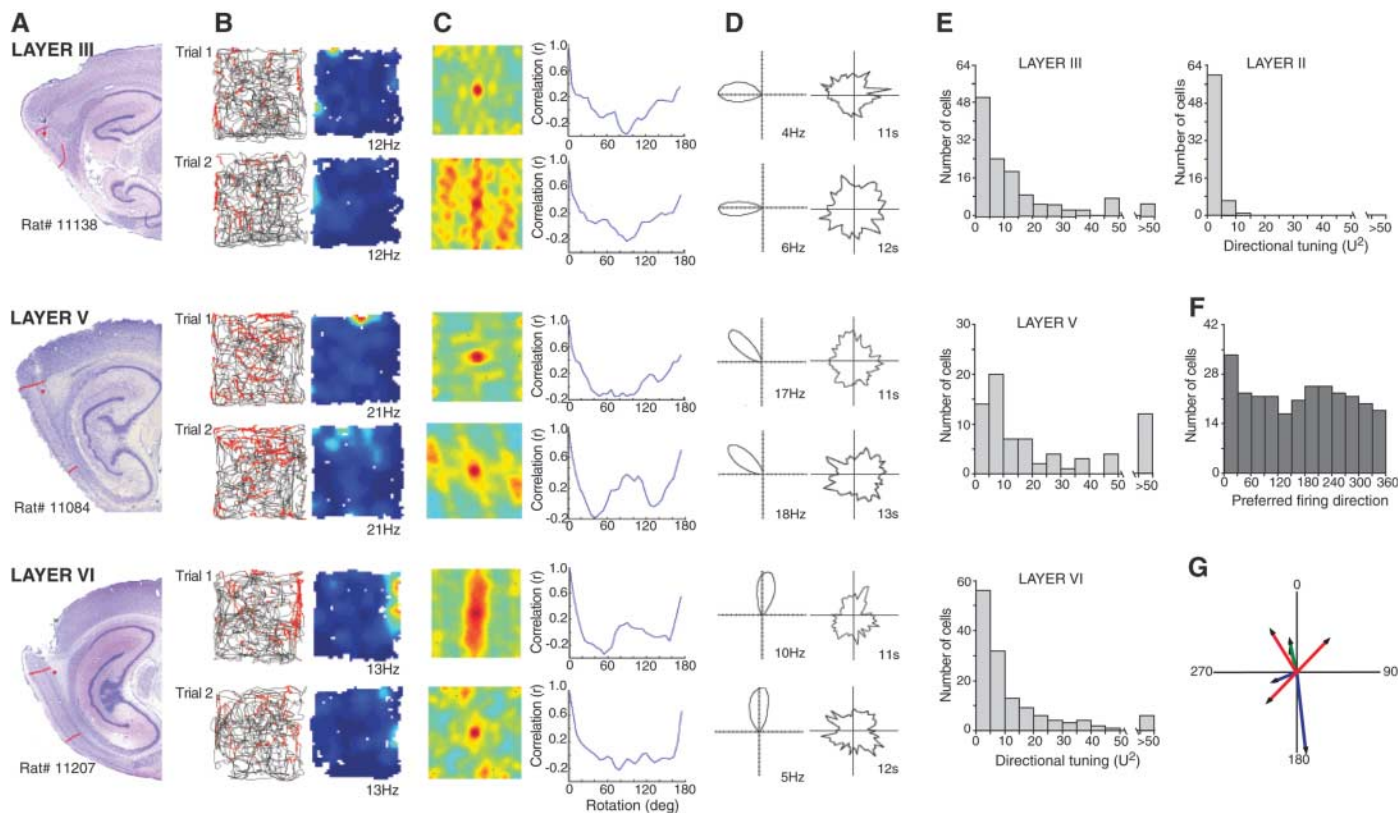


Fig. 2. Head-direction cells in the MEC. **(A)** Sagittal Nissl-stained sections from three rats showing recording locations in layers III, V, and VI. **(B)** Trajectory with spike locations (left) and color-coded rate maps (right) for three representative head-direction cells, one from each location in **(A)**. Two trials are shown. Symbols as in Fig. 1B. **(C)** Color-coded autocorrelation matrices (left) and periodicity of the autocorrelation (right) for the same three cells as in **(B)**. Note lack of periodicity. The correlation at 180° reflects the mirror symmetry of the autocorrelation matrix. Symbols and computations as in Fig. 1C. **(D)** Polar plots indicating strong directional tuning of firing rate in the cells shown in **(B)** and **(C)**. Left, firing rate as a function of head direction. Right, amount of time that the rat faced each

direction. Bin sizes were 6°. Peak firing rate and peak dwell time are indicated. Watson's U^2 values for these cells ranged from 23 to 33. **(E)** Frequency distribution of head-direction tuning for all cells recorded in all layers. Directional tuning is expressed by Watson's U^2 test statistic (19). **(F)** Distribution of peak firing direction relative to a common external reference for the entire sample of head-direction cells (all layers). **(G)** Vector representation of firing direction (angle) and firing rate (length) of 7 colocalized head-direction cells in layer VI (mean vectors for each cell). Cells from the same tetrode have the same color. There was no significant clustering of the mean vectors in this recording (Watson's U^2 test, $U^2 = 0.01$, critical value 0.18, n.s.) (see also fig. S5).

Grid cells and head-direction cells formed overlapping populations. The 2D distribution of gridness and directional tuning was continuous, such that some grid cells were directionally tuned and some head-direction cells had grid correlates (Fig. 3, A to D, and fig. S7). The proportion of grid cells with conjunctive properties was layer-dependent (table S1). The largest proportion was encountered in layers III and V, where 66% and 90% of the grid cells had dual response properties, respectively. In layer VI, the proportion was 28%. No conjunctive cells were observed in layer II. Differences between layers were significant (all four cell layers, $\chi(3) = 28.4$, $P < 0.001$; layers III to VI, $\chi(2) = 6.2$, $P < 0.05$). The degree of directional tuning in cells that met selection criteria for both gridness and directionality was not significantly different from that of pure head-direction cells (mean U^2 values, 18.0 and 19.4, respectively; $P > 0.05$) (Fig. 3, D and E). Cells with different degrees of gridness and directionality always responded as a coherent

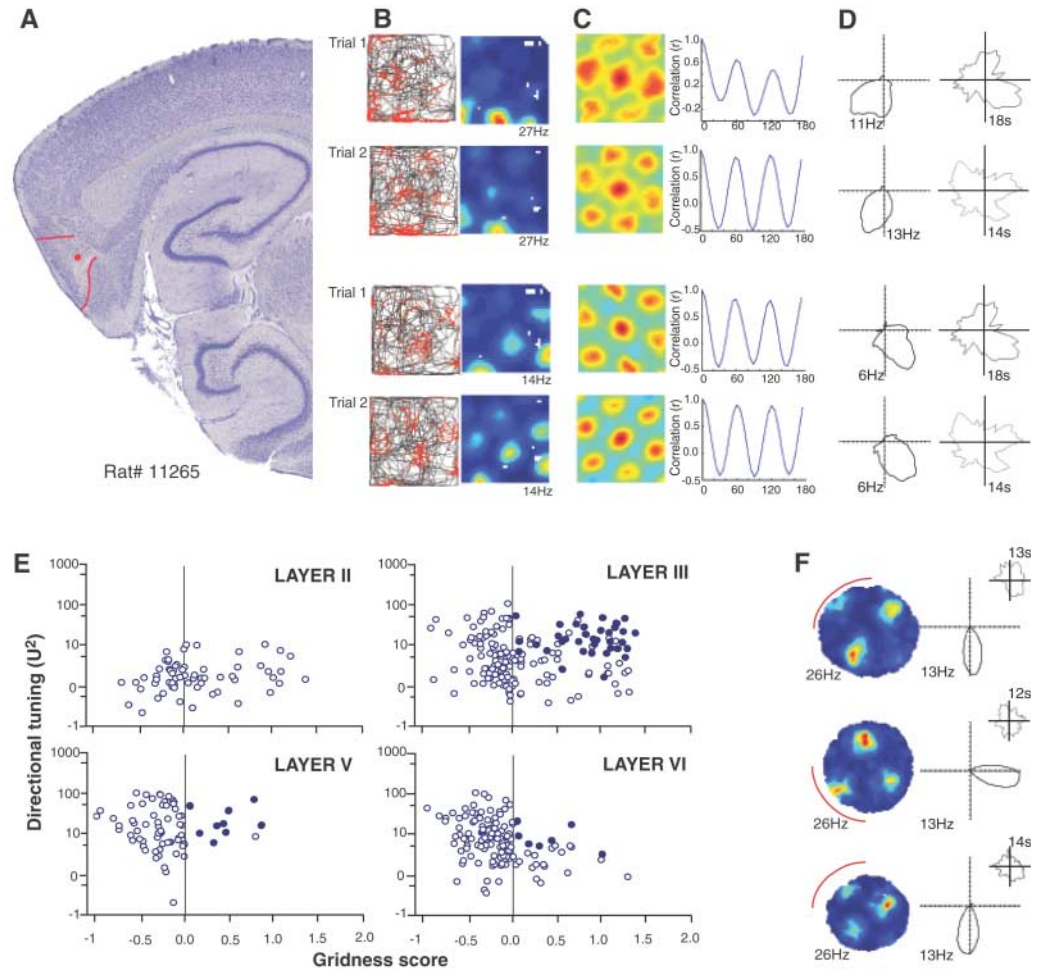
ensemble during environmental manipulations such as the rotation of a polarizing cue card (Fig. 3F and fig. S8) (22).

Cells with conjunctive grid and head-direction properties may update the representation of spatial location by integrating position and direction information as the animal moves around; however, translocation of the position vector between grid cells with shifted firing vertices may require additional information about the animal's instantaneous speed of movement (23–27). We thus asked whether speed was expressed in the firing rates of any of the cells that we recorded (Fig. 4). Because all position points were used in this analysis, including those outside the firing fields, the correlation between speed and rate was generally low (Fig. 4A). Yet, regression analyses showed a consistent positive speed-rate relation in nearly all grid cells (141/150 cells, $P < 0.001$), head-direction cells (153/220 cells, $P < 0.001$) and grid \times head-direction cells (45/53 cells, $P < 0.001$), suggesting that a substantial proportion

of the network expressed information about how fast the animal was moving (Fig. 4B). The slope of the regression line was steeper for conjunctive cells and grid cells than for head-direction cells [$F(2,422) = 5.5$, $P < 0.005$; conjunctive versus head-direction, $P = 0.009$; grid versus head-direction, $P = 0.01$; conjunctive versus grid, $P = 0.60$; Tukey HSD test). The y -intercept of the regression line was positive in 422 out of 423 cells (Fig. 4C). Average rates at the lowest velocity (0 to 3 cm/s) were 2.26 ± 0.03 Hz (grid cells), 2.50 ± 0.02 Hz (head-direction cells) and 2.39 ± 0.05 Hz (grid \times head-direction cells). Thus, grid structure and directional tuning can be maintained during brief stops along the rat's trajectory. Few stops were longer than 5 s.

These results imply that, despite the differential hippocampal and neocortical connections of superficial and deep layers of the MEC (10, 28), all layers together operate as an integrated unit, with considerable interaction between grid cells, present in all principal cell

Fig. 3. Conjunctive representation of position and direction. **(A to D)** Firing correlates of two simultaneously recorded cells with conjunctive grid and head-direction properties in layer III of MEC in one rat. Two trials are shown; note consistent discharge profile. **(A)** Sagittal Nissl-stained section showing recording location in layer III of the dorsocaudal MEC. **(B)** Trajectory with spike locations (left) and color-coded rate map (right). **(C)** Color-coded spatial autocorrelation matrix (left) and the periodicity of the matrix (right). **(D)** Polar plots showing directional tuning of firing rate (left) and distribution of dwell time across head directions (right). Symbols and computations as in Fig. 2, B to D. **(E)** Scatterplot showing relation between gridness (Fig. 1D) and degree of head-direction tuning (Watson's U^2 , logarithmic scale; Fig. 2E) in all cells for which head direction was tracked. Each circle refers to one cell. Filled circles indicate cells that passed criteria for conjunctive firing. Note the high proportion of conjunctive cells in layers III and V. **(F)** Rate map for a grid cell (left) and polar plot for a head-direction cell (right) recorded simultaneously in layer VI of MEC after rotation of a polarizing cue card on the wall of the circular environment (red arc). Top and bottom, cue card in original position. Middle panel, cue card rotated 90°. Insets show distribution of time across head directions. Three other head-direction cells were recorded simultaneously; all of these rotated 90° (fig. S8).



layers, and head-direction cells, present in layers III to VI. Principal neurons from layer II to layer V have apical dendrites that extend up to the pial surface (14, 29). Layer V cells have extensive axonal connections to the superficial layers (14, 15), and local axons of layer II and III cells may contact the dendrites of deeper cells (30). This implies that visuospatial and movement-related signals from the post-rhinal and retrosplenial cortices (10, 28) and directional signals from the dorsal presubiculum (18–20, 31–34) may activate the entire MEC circuit even when the axonal input is specific to one or a few layers.

The results show that the spatial map in MEC comprises both grid cells and head-direction cells. These cell types form a continuous population, with grid cells expressing variable degrees of directional modulation and head-direction cells expressing variable degrees of grid structure. Conjunctive representations among input variables appear in many theoretical models for neural systems that perform coordinate transformations, and similar conjunctions of head direction and location have been observed in some cells in the dorsal presubiculum (35). Analogous conjunctive cells may be involved

in the computation of head-centered coordinates from retinal-location and eye-position data (“gain fields”) in the posterior parietal cortex (36, 37) and in the continuous updating of head direction cells on the basis of conjunctions between current head direction and head angular velocity (38, 39). Our results suggest that, as the animal moves, the position vector may be updated through integration of position, direction, and speed signals in the grid-cell network (23–27). Conjunctive cells are likely to play a critical role in this process. The conjunctive cells are located predominantly in layers III and V, where principal neurons have extensive axonal projections to the grid-cell population in layer II (14, 15). The ability of superficial cells to read out signals carried by these axons may be critical for translating activity over the population of grid cells, i.e., between cells with a different spatial phase, in a manner consistent with the rat’s motion. The direction of translation may be determined by the head-direction input; the distance may be controlled by the speed modulation. In essence, this mechanism would perform path integration in the MEC network.

The integration of directional and positional information is strongly facilitated by the inter-

mingled localization of the grid cells and the head-direction cells and the distributed representation of spatial phase (7) and head orientation in these cell types. Within a diameter of a few hundred micrometers or less, the complete range of positions and distances appears to be represented. It remains to be determined whether the integration of position, direction, and velocity is confined to the local circuitry, as in the columns of the isocortex (40), or extends across the entire entorhinal sheet of grid cells, spanning all grid spacings.

References and Notes

1. J. O’Keefe, L. Nadel, *The Hippocampus as a Cognitive Map* (Clarendon Press, Oxford, 1978).
2. G. J. Quirk, R. U. Muller, J. L. Kubie, J. B. Ranck Jr., *J. Neurosci.* **12**, 1945 (1992).
3. A. D. Redish, D. S. Touretzky, *Hippocampus* **7**, 15 (1997).
4. A. D. Redish, *Beyond the Cognitive Map: From Place Cells to Episodic Memory* (MIT Press, Cambridge, 1999).
5. P. E. Sharp, *Hippocampus* **9**, 432 (1999).
6. M. Fyhn, S. Molden, M. P. Witter, E. I. Moser, M.-B. Moser, *Science* **305**, 1258 (2004).
7. T. Hafting, M. Fyhn, S. Molden, M.-B. Moser, E. I. Moser, *Nature* **436**, 801 (2005).
8. E. L. Hargreaves, G. Rao, I. Lee, J. J. Knierim, *Science* **308**, 1792 (2005).

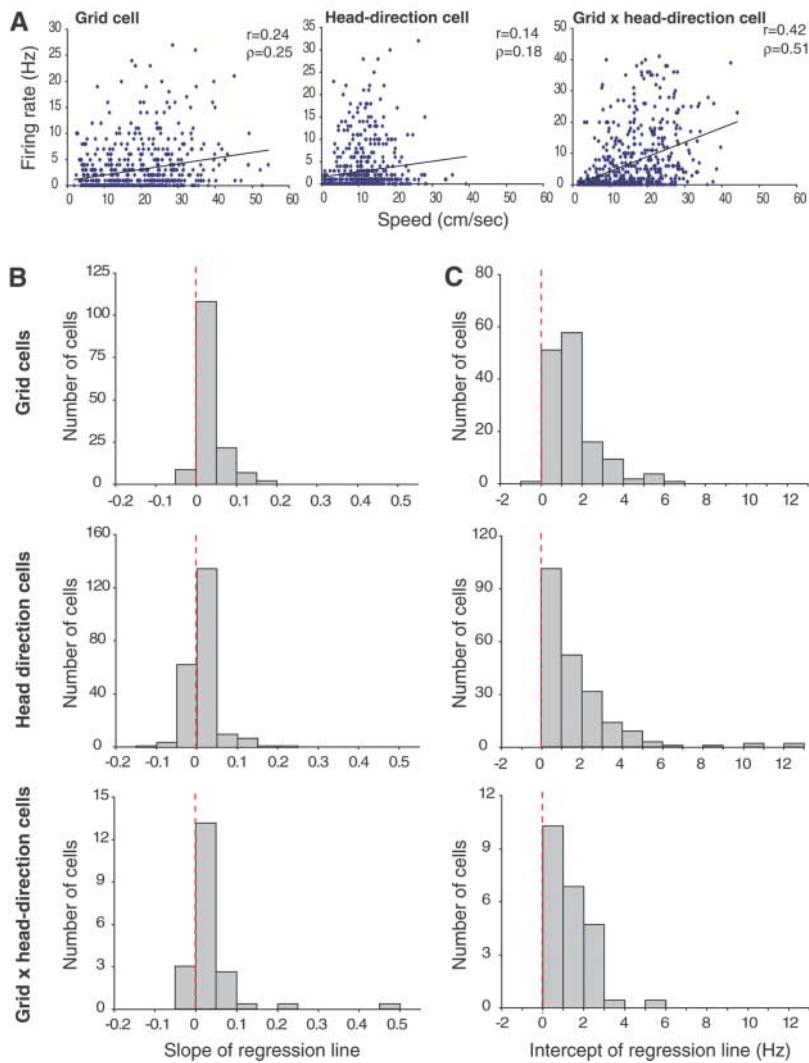


Fig. 4. Velocity modulation of grid cells, head-direction cells, and conjunctive cells. **(A)** Scatterplot showing relation between velocity and firing rate in three representative cells (grid cell, head-direction cell, and grid \times head-direction cell; one plot for each cell). Dots refer to individual spikes. Linear regression line and correlation values are indicated (Pearson's product-moment correlation and Spearman's rank correlation). **(B)** Frequency distribution for the slope of the rate/velocity function. Analyses were based on the entire set of videotracker positions, irrespective of whether they were inside or outside the positional or directional firing fields of the cell. Nearly all grid cells, head-direction cells, and grid \times head-direction cells had positive slope values, i.e., the firing rate increased with velocity. **(C)** Frequency distribution for the estimated firing rate at zero velocity (the y-intercept of the regression line). All cells except one had positive intercepts, implying that the activity of the network was not interrupted by brief stops on the rat's trajectory.

map (or its 2D autocorrelation function) come into correspondence with the unrotated map every 60° .

13. M. Fyhn, T. Hafting, A. Treves, M.-B. Moser, E. I. Moser, *Soc. Neurosci. Abstr.* **31**, 198.6 (2005).
14. T. van Haeften, T. L. Baks-te-Bulte, P. H. Goede, F. G. Wouterlood, M. P. Witter, *Hippocampus* **13**, 943 (2003).
15. F. Kloosterman, T. van Haeften, M. P. Witter, F. H. Lopes da Silva, *Eur. J. Neurosci.* **18**, 3037 (2003).
16. Materials and methods are available as supporting material on Science Online.
17. If this linear trend persists throughout the dorsal-to-ventral extent of MEC, it predicts grids with spacings of about 2 m in the most ventral portions of MEC.
18. J. S. Taube, R. U. Muller, J. B. Ranck Jr., *J. Neurosci.* **10**, 420 (1990).
19. J. S. Taube, *Prog. Neurobiol.* **55**, 225 (1998).
20. A. Johnson, K. Seeland, A. D. Redish, *Hippocampus* **15**, 86 (2005).
21. J. J. Knierim, H. S. Kudrimoti, B. L. McNaughton, *J. Neurosci.* **15**, 1648 (1995).
22. A similar coupling has been reported for thalamic head-direction cells and hippocampal place cells (21).
23. B. L. McNaughton *et al.*, *J. Exp. Biol.* **199**, 173 (1996).
24. K. Zhang, *J. Neurosci.* **16**, 2112 (1996).
25. A. Samsonovich, B. L. McNaughton, *J. Neurosci.* **17**, 5900 (1997).
26. J. O'Keefe, N. Burgess, *Hippocampus* **15**, 853 (2005).
27. M. C. Fuhs, D. S. Touretzky, *J. Neurosci.* **26**, 4266 (2006).
28. M. P. Witter, H. J. Groenewegen, F. H. Lopes da Silva, A. H. Lohman, *Prog. Neurobiol.* **33**, 161 (1989).
29. B. N. Hamam, T. E. Kennedy, A. Alonso, D. G. Amaral, *J. Comp. Neurol.* **418**, 457 (2000).
30. T. Iijima *et al.*, *Science* **272**, 1176 (1996).
31. M. Caballero-Bleda, M. P. Witter, *Exp. Brain Res.* **101**, 93 (1993).
32. T. van Haeften, F. G. Wouterlood, B. Jorritsma-Byham, M. P. Witter, *J. Neurosci.* **17**, 862 (1997).
33. Y. Honda, N. Ishizuka, *J. Comp. Neurol.* **473**, 463 (2004).
34. F. G. Wouterlood *et al.*, *Brain Res.* **1013**, 1 (2004).
35. F. Cacucci, C. Lever, T. J. Willis, N. Burgess, J. O'Keefe, *J. Neurosci.* **24**, 8265 (2004).
36. R. A. Andersen, G. K. Essick, R. M. Siegel, *Science* **230**, 456 (1985).
37. J. Xing, R. A. Andersen, *J. Cogn. Neurosci.* **12**, 601 (2000).
38. W. E. Skaggs, J. J. Knierim, H. S. Kudrimoti, B. L. McNaughton, in *Advances in Neural Information Processing Systems 7*, G. Tesoro, D. Touretzky, T. Leen, Eds. (MIT Press, Cambridge, 1995), pp. 173–180.
39. L. L. Chen, L. H. Lin, E. J. Green, C. A. Barnes, B. L. McNaughton, *Exp. Brain Res.* **101**, 8 (1994).
40. V. B. Mountcastle, *Brain* **120**, 701 (1997).
41. We thank S. Molden and A. Treves for discussion and A. M. Amundsgård, K. Haugen, K. Jenssen, E. Sjulstad, R. Skjerpeng, and H. Waade for technical assistance. This work was supported by a Centre of Excellence grant from the Norwegian Research Council.

Supporting Online Material

www.sciencemag.org/cgi/content/full/312/5774/758/DC1

Materials and Methods

Figs. S1 to S9

Table S1

30 January 2006; accepted 30 March 2006

10.1126/science.1125572

9. D. A. Nitz, *Neuron* **49**, 747 (2006).

10. M. P. Witter, D. G. Amaral, in *The Rat Nervous System, 3rd Edition*, G. Paxinos, Ed. (Academic Press, San Diego, 2004), pp. 637–703.

11. C. Parron, E. Save, *Exp. Brain Res.* **159**, 349 (2004).

12. The firing field of a grid cell has the form of a regular grid whose unit cell is a pair of inverted equilateral triangles or a rhombus with interior angles of 60° and 120° . Firing rate is maximal at the vertices of the grid and minimal at the center of each triangle. Rotations of the firing rate